Contour Integral Method with Fringe Complex Images for the Rapid Solution of Patch Resonators of Arbitrary Shape

Amjad A. Omar, Y. L. Chow, and M. G. Stubbs

Abstract—**An accurate and computationally efficient method is presented for solving patch resonators of arbitrary shape. This method improves on Okoshi's 2-D contour integral (CI) method by including the fringe fields and radiation, through use of the 3-D complex images. The presented method may be called contour integral with fringe (CIF). Experiments are conducted to verify the accuracy of the CIF method and show very good agreement with the theoretical predictions.**

I. Introduction

RECENTLY, filters composed of patch resonators have attracted much attention because of their appealing properties. Their lightweight and high quality factors, especially if built of superconducting materials [1], are very attractive for satellite communications.

The use of patch filters necessitates the accurate modeling of the patch resonator shown in Fig. 1(a). This modeling should include the fringe fields and radiation, and place no restriction on the shape of the patch. It should also be computationally efficient to prepare for the design of larger filter circuits containing more than one patch [1].

Four methods have frequently been used to solve patch resonators: 1) The mode matching method [2] expands the fields under the patch in terms of a finite number of modes. This method can therefore only solve patches of regular shapes that have known modal expansions. 2) The point-matching method [3] matches the field on the large surface of the patch. This results in the matrix of electric current having frequently between 180 to 600 unknowns for one single patch. This method is thus unsuitable for solving large circuits of more than one patch, and also has difficulty with patches having mode coupling stubs [1]. 3) The spectral domain method [4] requires the basis functions for the electric current on the patch to satisfy the edge condition on the patch and be analytically fourier transformable. This, however, is difficult to achieve for patches of irregular shapes having mode coupling stubs. 4) The 2-D contour integral (CI) method of Okoshi [5] matches only around the perimeter (edge) of the patch. This method places no restriction on the shape of the patch and produces a 3 to 20-fold reduction in unknowns. However, the CI method assumes a magnetic wall around the edge of the patch, thereby ignoring the effect of the fringing fields and the radiation. This magnetic wall assumption has to be relaxed for more accurate simulation of the patches, and also to include the coupling between adjacent patches. Martinson and Kuester [6] proposed a fringe correction factor depending on the substrate ϵ_r. Such an improvement still ignores the dependence of the fringing fields on the contour of the edges. Therefore, an alternative improvement on the CI method is desirable. One such improvement is proposed below.

The resonator structure is divided into the interior and exterior regions, as shown in Fig. 1(b). For the interior, we use the *2-D contour integral (CI) method*. However, unlike the standard CI method, we do not assume a magnetic wall of zero tangential magnetic field on the patch perimeter. Instead, we match both the electric and magnetic fields between the interior and exterior regions. The fields for the exterior region, which account for the fringe fields and radiation, are derived using the accurate and rapidly convergent complex image technique [7]. The proposed method, similar to the CI method, is general for any patch shape, and highly convergent, as it only discretizes the perimeter of the patch. It is also more accurate, as it includes the fringe field and radiation.

With the addition of the fringe field through the 3-D complex images, the method of this paper is named *contour integral with fringe (CIF)*.

Experiments were conducted on rectangular, circular, and dual mode patches (rectangular with corner cut) to verify the accuracy of the CIF method.

Section II explains the theoretical background of this paper. This includes derivation of the CI method through the use of vector potentials, and the complex image Green's functions. Section III explains the theoretical contribution of this paper of matching the fields at the patch perimeter. Section IV-A explains our choice of the moment method type and basis functions. Section IV-B presents numerical and experimental results for directly fed microstrip patches having rectangular and circular shapes, as shown in Fig. 2(a) and (b). Results are also presented for a square patch with a corner cut [Fig. 2(c)]. Section V presents our conclusion.

The focus of this paper is on the directly fed patch resonators. Gap-coupled patches, as well as coupling between different patches, will be studied in the future.

Manuscript received May 27, 1994; revised May 25, 1995.

A. A. Omar is with the Department of Electrical Engineering, Amman University, Jordan.

Y. L. Chow is with the Department of Electrical Engineering, University of Waterloo, Canada.

M. G. Stubbs is with the Communications Research Centre, Ottawa, Canada.

IEEE Log Number 9413404.

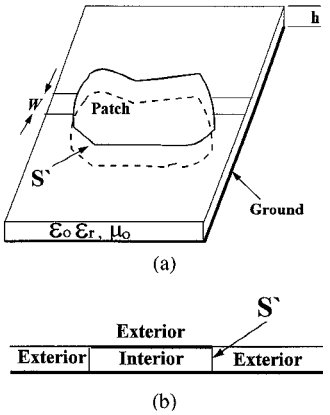

Fig. 1. The microstrip patch resonator with direct microstrip feed: (a) 3-D view. (b) Cross section. (w is the width of the feed microstripline).

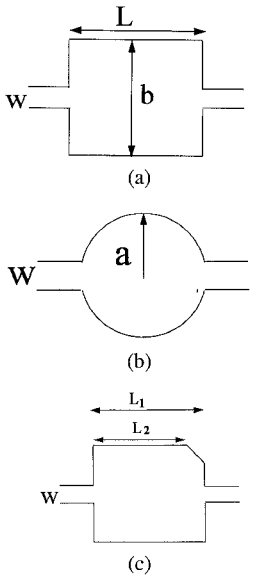

Fig. 2. Microstrip patch resonators of different shapes: (a) Rectangular patch. (b) Circular patch. (c) The dual mode square patch with corner cut.

II. Theoretical Background

As background, this section outlines separately each of the two methods, contour integral and complex images. The combination of the two methods on the patch perimeter (to satisfy the boundary conditions on the perimeter) will be explained in Section III-A.

A. Standard Contour Integral (CI) Method—A 2-D Formulation for the Interior Region

For the interior region, the fields are assumed to be invariant along the substrate thickness. This allows the use of the 2-D contour integral (CI) method [5] to relate the electric voltage (magnetic current) on the whole boundary of the interior region I^m_{inte} to the equivalent electric current I^e_{inte} on this boundary.

The CI (Okoshi's) admittance matrix has been derived in the literature [5] using Green's theorem. Equivalently, in this section, the same matrix is derived from vector potentials of both electric and magnetic currents.

The electric voltage along the perimeter of the patch (at any location s), resulting from both longitudinal electric and transverse magnetic currents in a 2-D problem (no variation with z) as shown in Fig. 3(a), is given by [8]

$$V^e(s) = -hE_z(s) = j\omega\mu_0 hA_z(s) + h(\vec{\nabla} \times \vec{F}).\hat{z} \quad (1)$$

where V^e, E_z, A_z, $\vec{F}$ are the electric voltage, the z-directed electric field component, the electric current vector potential in the z-direction, and the magnetic current vector potential tangent to the perimeter in the transverse plane, respectively, and h is the microstrip substrate thickness. In (1), the contribution from the electric scalar potential (resulting from the electric charge), is not included since its derivative with respect to z is zero. In general, for a 2-D problem with no variation along z-axis

$$A_z(\vec{s}) = \frac{1}{2j}\int_C J^e_{\text{inte}}(\vec{s}')H_0^{(2)}(k_d|\vec{s} - \vec{s}'|)\,ds' \quad (2)$$

$$\vec{F}(\vec{s}) = \frac{1}{2j}\int_C J^m_{\text{inte}}(\vec{s}')\hat{a}_m H_0^{(2)}(k_d|\vec{s} - \vec{s}'|)\,ds' \quad (3)$$

$$(\vec{\nabla} \times \vec{F}).\hat{z} = -\frac{1}{2j}\int_C J^m_{\text{inte}}(\vec{s}')\frac{d}{d|\vec{s} - \vec{s}'|}[H_0^{(2)}(k_d|\vec{s} - \vec{s}'|)] (\hat{a}_m \times \hat{r}).\hat{z}\,ds' \quad (4)$$

where J^e_{inte} and J^m_{inte} are the equivalent electric and magnetic current densities, respectively, radiating in the interior region; $\hat{a}_m$, $\hat{r}$, $\hat{z}$ are unit vectors, respectively, in the direction of the magnetic current at the source s', pointing from the source to the field, and in the z-direction. k_d is the wave number in the dielectric, and $H_0^{(2)}$ is the Hankel function of the second kind of order zero. The triple product in (4) is given by

$$(\hat{a}_m \times \hat{r}) \cdot \hat{z} = \cos\theta \quad (5)$$

where θ is the angle between the normal to the perimeter at s' and the straight line joining the source point s' to the field point s [5]. Substituting (2)–(5) in (1) yields the standard Okoshi integral equation of the interior region, relating the edge (equivalent) magnetic current (electric voltage) I^m_{inte} to the edge (equivalent) electric current density J^e_{inte}

$$I^m_{\text{inte}} = \frac{1}{2j}\int_C \{k_d \cos\theta H_1^{(2)}(k_d|\vec{s} - \vec{s}'|)I^m_{\text{inte}}(\vec{s}') + j\omega\mu_0 hH_0^{(2)}(k_d|\vec{s} - \vec{s}'|)J^e_{\text{inte}}(\vec{s}')\}\,ds' \quad (6)$$

where I^m_{inte} is the equivalent magnetic current on the perimeter of the interior region, $H_1^{(2)}$ represents the Hankel function of the second kind of order one, and C is the contour of the patch. Rearranging (6), with the electric current and edge magnetic current to different sides of the equal sign, gives the following matrix equation

$$\underline{I}^e_{\text{inte}} = [Y_{\text{inte}}]\underline{I}^m_{\text{inte}} \quad (7)$$

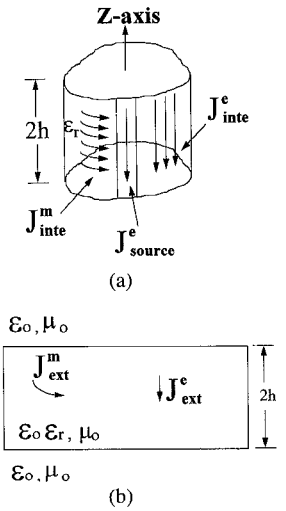

Fig. 3. Splitting the resonator structure into interior and exterior regions. (a) The interior homogeneous 2-D region. (b) The exterior region in a dielectric substrate of thickness $2h$.

where I^e_{inte} is the column matrix of the (edge) electric current in the interior region, and $[Y_{\text{inte}}]$ is the standard 2-D Okoshi admittance matrix. The final expression for the interior admittance elements $[Y_{\text{inte}}]$ can be obtained from [5].

It is important to emphasize that the CI (Okoshi) matrix equation in (7) relates the electric current to the magnetic current on the whole perimeter of the patch, with the only assumption being that the fields are invariant along the substrate thickness. However, in solving (7), the CI method assumes that the electric current (related to the tangential magnetic field) is nonzero only at the port (feed) locations, thereby ignoring the fringe fields and radiation. This assumption is removed in our formulation of the CIF method where we match both the electric and magnetic fields in the interior and exterior regions along the whole perimeter of the patch, as explained in Section III-A.

B. Complex Images—A 3-D Formulation of the Exterior Region

Similar to the electric field in (1), the magnetic field required here for the exterior region, also results from both the electric and magnetic currents radiating in a dielectric substrate [Fig. 3(b)]. Since the effect of the 3-D fringe field is usually small, and since this effect is predominantly due to the edge magnetic current I^m_{ext}, we have neglected without significant error the contribution of the electric current I^e_{ext}. Therefore, the magnetic field component tangent to the perimeter in the exterior region, is given by

$$H_t^{\text{ext}} = -j\omega\epsilon_0\epsilon_r \vec{F} \cdot \hat{a}_m - \vec{\nabla}\Phi_m \cdot \hat{a}_m. \tag{8}$$

The expressions for (the magnetic current) vector potential $\vec{F}$, and the (magnetic charge) scalar potential Φ_m, are derived using the complex image technique [9].

In the complex image technique, the effect of the dielectric medium is simulated by a set of images which have complex amplitudes and complex locations. These images are highly convergent and accurate such that only four complex images are sufficient to produce less than 0.5% error in the Green's functions [9]. This technique also allows the separation of the contribution of the surface waves. The expressions for the (magnetic current) mixed potentials (F_t and Φ_m) are the dual of the corresponding electric current mixed potentials given in [9]. Hence, when converted, (8) gives the following matrix equation

$$\underline{I}^e_{\text{ext}} = -[Y_{\text{ext}}]\underline{I}^m_{\text{ext}} \tag{9}$$

where I^e_{ext}, I^m_{ext} are column matrices for the edge electric and magnetic currents, respectively, radiating in the exterior region, and $[Y_{\text{ext}}]$ is the 3-D exterior complex image admittance matrix defined in [10]. The minus sign in (9) is added so that the definition of $[Y_{\text{ext}}]$ in (9) conforms with the standard definition given in [10], [11].

III. Theory

This section presents the contribution of this paper of combining the contour integral method of Section II-A with the complex images of Section II-B to satisfy the boundary conditions on the patch perimeter.

A. Our Method (CIF)—A Combination of the 2-D CI Method and the 3-D Complex Images

In solving the CI matrix equation (7), the CI method forces the tangential magnetic field to vanish on the patch perimeter. Our method matches the tangential E- and H-fields on the patch perimeter of the interior region to the corresponding fields of the exterior region, as follows

1) Tangential E-Fields: Let the tangential electric field on the perimeter of the patch in the interior and exterior regions be $\vec{E}^p_{\text{inte}}$, $\vec{E}^p_{\text{ext}}$. Hence, the equivalent magnetic current density on the perimeter of the interior region J^m_{inte} is given by

$$J^m_{\text{inte}} = -\hat{n}\text{x}\vec{\text{E}}^{\text{p}}_{\text{inte}} \cdot \hat{\text{a}}_{\text{m}} \tag{10}$$

where $\hat{n}$ is a unit vector normal to the perimeter of the patch pointing toward the inside, and $\hat{a}_m$ is a unit vector tangent to the perimeter in the direction of I^m_{inte}. With $\hat{n}$ defined as above, the magnetic current density on the perimeter of the exterior region J^m_{ext} is given by

$$J^m_{\text{ext}} = \hat{n}\text{x}\vec{\text{E}}^{\text{p}}_{\text{ext}} \cdot \hat{\text{a}}_{\text{m}}. \tag{11}$$

Since the tangential E-field is continuous on the patch perimeter (i.e, $\vec{E}^p_{\text{inte}} = \vec{E}^p_{\text{ext}}$), therefore from (10) and (11) we get, after converting the current densities to currents

$$I^m_{\text{inte}} = -I^m_{\text{ext}} = I^m. \tag{12}$$

Equation (12) matches the tangential electric field across the patch perimeter.

2) Tangential H-Fields: Let the tangential magnetic fields on the perimeter of the patch in the interior and exterior regions be $\vec{H}_{\text{inte}}$, $\vec{H}_{\text{ext}}$, respectively. From the equivalence principle, the equivalent electric currents on the perimeter of the interior and exterior regions, J^e_{inte}, J^e_{ext}, are given in terms of the

magnetic fields in these regions, as follows

$$J^e_{\text{inte}} = \hat{n}\text{x}\vec{\text{H}}_{\text{inte}} \cdot \hat{\text{z}} \tag{13}$$

$$J^e_{\text{ext}} = -\hat{n}\text{x}\vec{\text{H}}_{\text{ext}} \cdot \hat{\text{z}} \tag{14}$$

where the magnetic fields in (13) and (14) are functions of the magnetic current densities J^m_{inte}, J^m_{ext} of (10) and (11), and $\hat{n}$ is defined in (10).

Expressing the excitation electric current density J^e_s, shown in Fig. 3(a), as the difference between the exterior and interior magnetic fields, and substituting (13) and (14) in the resultant equation gives

$$J^e_s = [\hat{n}\text{x}(\vec{\text{H}}_{\text{inte}} - \vec{\text{H}}_{\text{ext}})] \cdot \hat{\text{z}} = \text{J}^{\text{e}}_{\text{inte}}(\text{J}^{\text{m}}_{\text{inte}}) + \text{J}^{\text{e}}_{\text{ext}}(\text{J}^{\text{m}}_{\text{ext}}) \tag{15}$$

where J^e_{inte} is defined in (7), while J^e_{ext} is defined in (9). Finally, on substituting (7) and (9) in (15), and converting the current densities to currents, we get the matrix equation

$$I^e_s = \{[Y_{\text{inte}}] + [Y_{\text{ext}}]\}I^m = \{[Y_{\text{inte}}] + [Y_{\text{ext}}]\}V^e. \tag{16}$$

In (16), $I^e_s$is the vector excitation electric current pointing from the patch to ground, as shown in Fig. 3, and V^e is the vector of voltage to ground along the patch perimeter.

Equation (16) summarizes our method, which combines the CI method (represented by $[Y_{\text{inte}}]$), with the 3-D complex images (represented by $[Y_{\text{ext}}]$). The 3-D complex image matrix has been shown [9], [10] to accurately account for the fringe field and physical radiation.

IV. Numerical Results

A. Choice of Basis Functions

Throughout the different numerical tests conducted on patches of different shapes, Galerkin's moment method with triangular basis functions produced results that are signficantly closer to experiment than those of the point matching moment method with pulse basis functions. The latter is usually used with the original CI method of Okoshi [5]. The elements of $[Y_{\text{inte}}]$ for the Galerkin moment method with triangular basis functions are constructed from three triangularly weighted pulse functions in [11], while the corresponding elements for point matching are constructed from the simple expressions in [5]. The comparison between the two methods is illustrated in Fig. 4 for the rectangular patch of Fig. 2(a). With the accuracy verified in Fig. 4, the Galerkin moment method with triangular basis functions is employed throughout the remainder of this paper.

B. Comparisons Between the CI, CIF Methods, and Experiment

To demonstrate the accuracy and versatility of the CIF method, it is applied to solve the directly fed microstrip rectangular and circular patches [Fig. 2(a)–(b), respectively], and the dual mode square patch with corner cut [Fig. 2(c)].

The experimental results presented for comparison were obtained in our laboratory using an HP-8510 Network Analyzer. The effect of the discontinuity at the connectors was removed using the TRL calibration method.

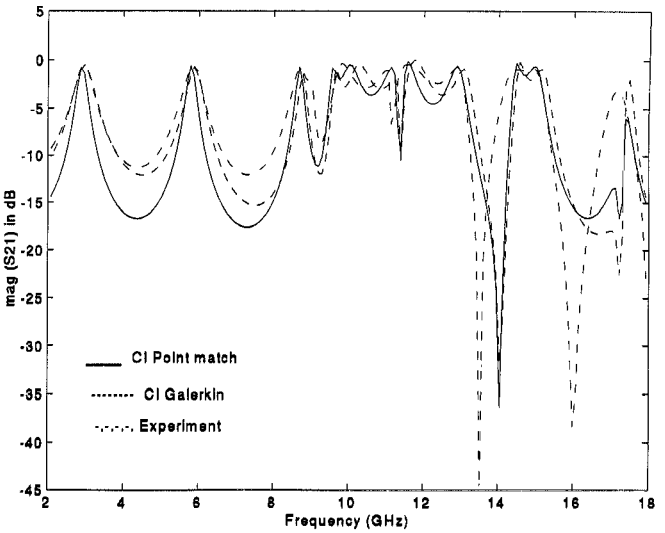

Fig. 4. $|S_{21}|$ for the rectangular patch resonator of Fig. 2(a), obtained using: 1) The CI method with Galerkin moment method and triangular basis functions. 2) The CI method with point matching moment method and pulse basis functions. 3) Experiment. ($L = 16.5$ mm, $b = 10$ mm, $W = 0.58$ mm, $h = 0.635$ mm, $\epsilon_r = 10$).

At low frequencies, where the resonances are widely separated (below 10 GHz), Figs. 5 and 7 for the rectangular and dual mode patches, respectively, show that the results obtained using the different methods (CI and CIF) are all in good agreement with experiment. There is a maximum difference in the amplitude of S_{21} of about 2 dB for the CIF method and 3 dB for the CI method. There are also only small shifts in the resonant frequencies (peaks of $|S_{21}|$) and null frequencies (minima of $|S_{21}|$). Fig. 6 for the circular patch, however, shows that the results from the CIF method are even closer to those of the experiment, both in amplitude, resonant, and null frequency locations, than the results from the CI method. For example, a round 6 GHz in Fig. 6(a), the resonant frequency obtained using the CI method is 8% above the resonant frequency obtained by the experiment. However, the resonant frequency using the CIF agrees almost perfectly with that of the experiment. The same applies for the resonance around 9.7 GHz.

At high frequencies, where the resonances are closely separated (above 10 GHz), Figs. 5 and 6 for the rectangular and circular patches, respectively, show that our CIF method produces results that are in better agreement with experiment. In Fig. 6 for the circular patch, the first null frequency of S_{21} ($\sim$ 10.5 GHz) obtained by the CI method is 10.6% above the experiment's first null, while the null frequency obtained by the CIF matches perfectly that of the experiment. Also, the second null frequency of S_{21} ($\sim$14.5 GHz) obtained by the CI method is 10.5% above that of the experiment, while using the CIF the null is only about 0.7% above the experiment. Also, the resonant frequencies (peaks of S_{21}) obtained using the CIF method match perfectly those of the experiment, while those obtained using the CI are above the experiment by about 2.5%.

As for the results of the dual mode patch of Fig. 7, we found it more convenient to display our results only up to 10 GHz because the null frequencies above that are too closely

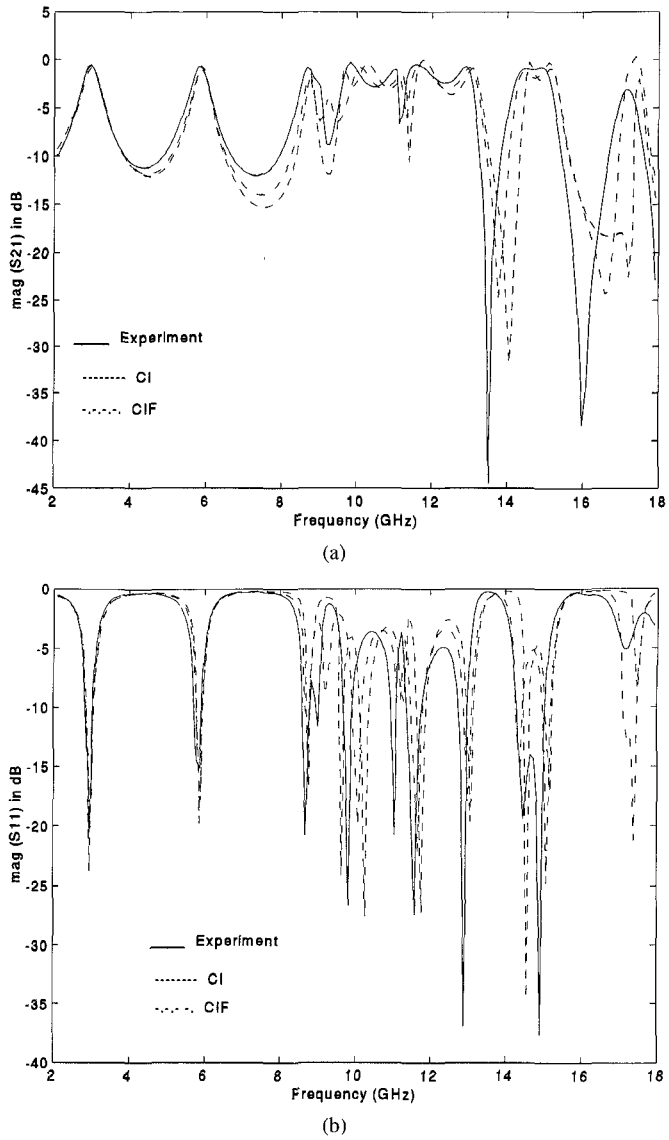

Fig. 5. A comparison between the S-parameters obtained using the CI, CIF methods, and our experiment, for the *rectangular* patch resonator of Fig. 2(a): (a) $|S_{21}|$. (b) $|SV_{11}|$. (Dimensions are in Fig. 4).

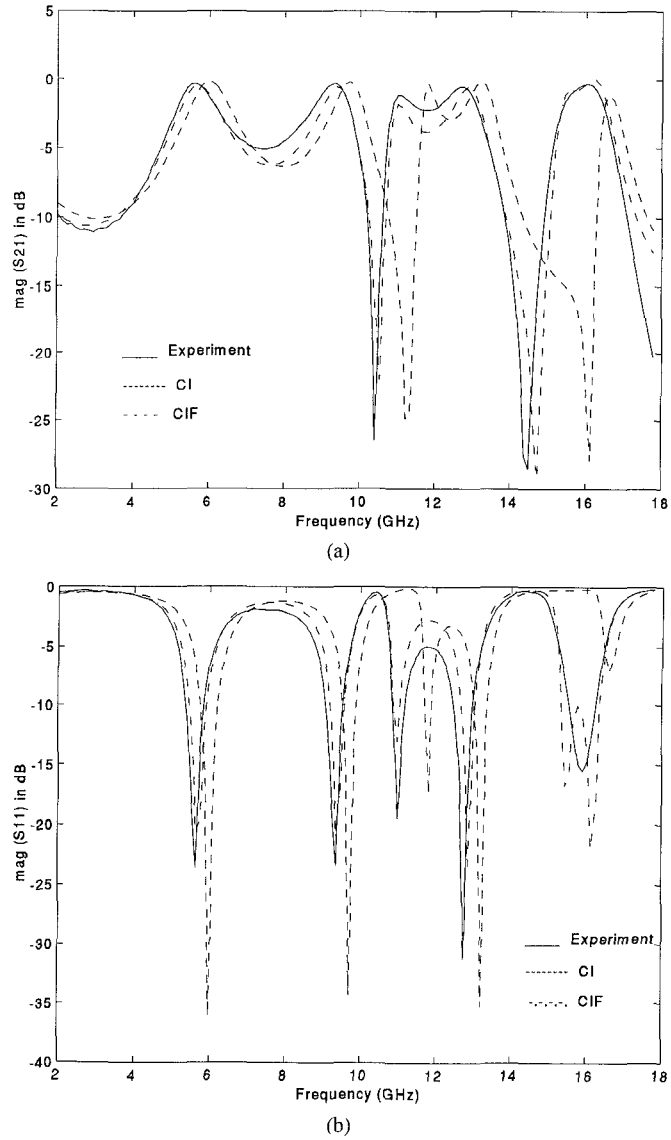

Fig. 6. A comparison between the S-parameters obtained using the CI, CIF methods, and our experiment, for the *circular* patch resonator of Fig 2(b): (a) $|S_{21}|$. (b) $|S_{11}|$. ($a = 5$ mm, $W = 0.58$ mm, $h = 0.635$ mm, $\mathcal{E}_r = 10$).

spaced. At the lower end of the displayed frequency range, which corresponds to the region of single mode operation of this patch (below 5 GHz), the maximum difference in the amplitude of S_{21} is only less than 1 dB. At the upper end, the maximum difference in the amplitude of S_{21} is about 5 dB.

From the discussion above, it becomes clear that adding the fringe fields and radiation is definitely improving the response at high frequencies and frequently even at low frequencies (Fig. 6). This improvement is more significant at the null frequency locations and for the "skirt" between the resonances.

To demonstrate the convergence of this approach, our results for the circular patch of Fig. 6 are compared with results obtained using the point matching software "Sonnet," as shown in Fig. 8. In this comparison, the CIF used only 40 segments along the peripheral of the patch while Sonnet used about 500 segments on the top surface of the patch. Choosing more segments in our method (up to 300) caused no detectable change in our results. In general, our results are found to be as accurate or more accurate than Sonnet's although we reduced the number of unknowns by about 10 folds. This could represent an important time and memory reduction, especially when dealing with large circuits having more than one patch [1]. It may also be important to point out that the strange behavior of the Sonnet curve at about 16.4 GHz may be caused by a box resonance. With open space assumed, our method has no such limitation.

V. Conclusion

In this paper, we have developed an accurate method for solving directly fed microstrip patches of arbitrary shape. This method improves on the contour integral (CI) method by including the fringe fields and the physical radiation of the patches using full wave complex image Green's functions. The

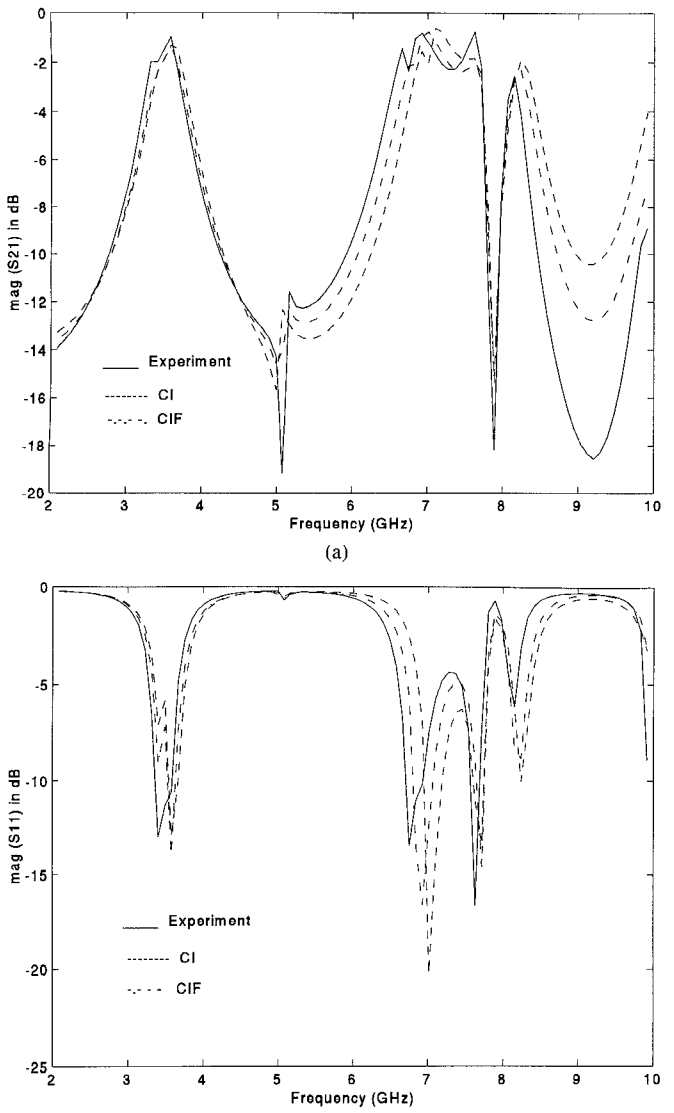

Fig. 7. A comparison between the S-parameters obtained using the CI, CIF methods, and our experiment, for the *dual mode square* patch resonator with corner cut of Fig. 2(c)L: (a) $|S_{21}|$. (b) $|S_{11}|$. ($L_1 = 13.9$ mm, $L_2 = 11.097$ mm, $W = 0.58$ mm, $h = 0.635$ mm. $\mathcal{E}_r = 10$).

accuracy has been demonstrated by several comparisons with the experimental results obtained in our laboratory.

The proposed method has been shown to be versatile in the sense that it can solve patches of any shape. It is also rapidly convergent, since it requires less than 50 segments around the patch perimeter. This results in two minutes per frequency point on a 33 MHz 80386 PC to solve any of the patches in Fig. 2. This represents a substantial reduction in computing time over the point matching and mode matching methods, with no sacrifice of accuracy. Results are obtained for the circular patch using the point matching software "Sonnet." In solving this patch, Sonnet software used 500 segments on the surface, while we only used 40 segments on the peripheral of the circular patch. When compared with experiments, our results are even found to be more accurate than those of Sonnet.

The above CIF method of modeling the fringe field and radiation of the patch as a 3-D closed loop of magnetic current

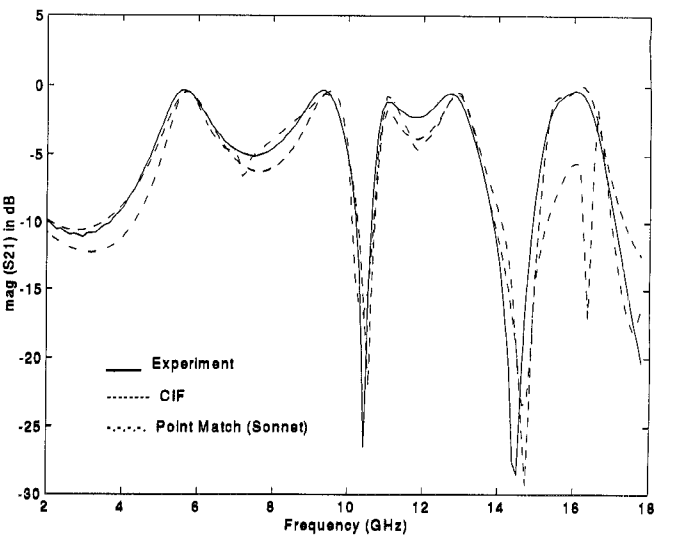

Fig. 8. A comparison between $|S_{21}|$ obtained using the CIF method, the point matching software "Sonnet" and with experiment for the circular patch with dimensions given in Fig. 6.

has been found to be accurate provided that the thickness of the microstrip substrate is less than $\lambda_d/15$ in the substrate. Accurate results were obtained even for substrate thicknesses as large as $\lambda_d/10$ for the circular patch. Within the thickness limit, our modeling of the patch can evidently be extended to the studies of gap excitation of patch and edge coupling between patches. Future work will be directed to these areas.

ACKNOWLEDGMENT

The authors would like to thank Dr. R. Faraji-Dana from the University of Waterloo and Dr. R. Mongia from CRC for the helpful discussions.

REFERENCES

[1] J. A. Curtis and S. J. Fiedziuszko, "Miniature dual mode microstrip filters," in *IEEE MTT-S Dig.*, 1991, pp. 443–446.
[2] G. D'Inzeo, F. Giannini, C. M. Sodi, and R. Sorrentino, "Method of analysis and filtering properties of microwave planar networks," *IEEE Trans. Microwave Theory Tech.*, vol. MTT-26, no. 7, pp. 462–471, July 1978.
[3] K. A. Michalski and D. Zheng "Analysis of microstrip resonators of arbitrary shape," *IEEE Trans. Microwave Theory Tech.*, vol. 40, no. 1, pp. 112–119, Jan. 1992.
[4] T. Itoh and W. Menzel, "A full-wave analysis method for open microstrip structures," *IEEE Trans. Antennas Propagat.*, vol. 29, no. 1, pp. 63–68, Jan. 1981.
[5] T. Okoshi, *Planar Circuits.* New York: Springer-Verlag, 1985. pp. 44–51.
[6] T. M. Martinson and E. F. Kuester, "Accurate analysis of arbitrarily shaped patch resonators on thin substrates," *IEEE Trans. Microwave Theory Tech.*, vol. 36, no. 2, pp. 324–331, Feb. 1988.
[7] A. A. Omar and Y. L. Chow, "A solution of coplanar waveguide with air-bridges using complex images," *IEEE Trans. Microwave Theory Tech.*, vol. 40, no. 11, pp. 2070–2077, Nov. 1992.
[8] R. F. Harrington, *Time Harmonic Electromagnetic Fields.* New York: McGraw-Hill, 1961, pp. 106–130.
[9] A. A. Omar and Y. L. Chow, "Complex image Green's functions for coplanar waveguides," in *IEEE AP-S Dig.*, 1992, pp. 1496–1499.
[10] A. A. Omar, "An Accurate Solution of 3-D Coplanar Waveguide Circuits," Ph.D. dissertation, University of Waterloo, 1993.
[11] R. F. Harrington, *Field Computation by Moment Method.* Malabar, FL: Krieger, 1968, pp. 62–81 and pp. 48–49.

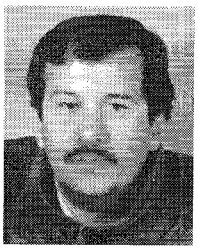

Amjad A. Omar was born in Kuwait in 1963. He received the Ph.D. degree in electrical engineering from the University of Waterloo, Canada in 1993. He obtained the M.Sc. and B.Sc. degrees in 1988 and 1985, respectively.

From May 1993 to August 1994, he was working as a Visiting Post Doctoral Fellow at the Communications Research Center in Ottawa, Canada. He is currently working as an Assistant Professor at Amman University in Jordan. His current research interests are in the numerical solution of microwave and millimeter wave integrated circuits, multilayered antennas, and in superconductivity.

Y. L. Chow, photograph and biography not available at the time of publication.

M. G. Stubbs, photograph and biography not available at the time of publication.